ADVANCED FUNCTIONAL MATERIALS
www.afm-journal.de

Materials Views
www.MaterialsViews.com

Porous Silicon Films Micropatterned with Bioelements as Supports for Mammalian Cells

*Martin J. Sweetman, Maurizio Ronci, Soraya Rasi Ghaemi, Jamie E. Craig, and Nicolas H. Voelcker**

Porous silicon (pSi) surfaces have been chemically patterned via a UV initiated hydrosilylation reaction of an alkene through a photomask, introducing chemical functionality in the exposed surface areas. A secondary, UV initiated hydrosilylation reaction with a second alkene of different functionality is performed to backfill the silicon hydride terminated regions on the surface, thereby affording patterned porous films with dual, surface chemistry. UV initiated hydrosilylations were performed using the alkene undecylenic acid N-hydroxysuccinimide (NHS) ester, and the pSi surfaces were stabilized by a second hydrosilylation reaction with a polyethylene glycol (PEG) appended alkene. NHS ester and PEG functionalized surfaces were used for the selective immobilization of the cell adhesion mediator protein fibronectin (FN), in the NHS-functional regions. Matrix-assisted laser desorption/ionization mass spectrometry imaging on the protein functionalized pSi surface confirmed the patterned conjugation of the FN to the NHS functionalized regions. Mammalian cells cultured on these surfaces showed attachment that was confined to the patterned areas of FN on the pSi surface.

1. Introduction

The unique chemical and physical properties of porous silicon (pSi) have been the target of manifold studies pursuing applications in biological and chemical sensing, tissue culture systems, drug release and optoelectronic devices.[1–7] pSi is prepared ('etched') by anodization in the presence of hydrofluoric acid (HF) and a surfactant. The porosity and pore diameter and pore depth of pSi can be tuned by simply varying the etching parameters.[8,9] A key advantage of pSi in biological applications is the fact that it is degradable in aqueous milieu and that the degradation product is non-toxic silicic acid.[10] As a consequence, pSi can be used for both in vitro and in vivo biological applications.[11,12] Along with the good biocompatibility, pSi also has unique optical properties that allow biological and chemical interactions within the porous matrix to be monitored in real time.[7,13,14] These unique traits of pSi have allowed the development of highly specialized biosensors that are able to assess specific cellular functions, such as apoptosis and enzyme excretion.[15,16]

Another crucial aspect for pSi based sensors and devices is the ability to selectively control the surface chemistry within the porous structure. Incorporating desired chemical functionality into the porous layer has been an area of extensive research endeavour and a range of different functionalization methods have been reported.[17–21] The most common surface modification procedures for pSi by far are silanization and hydrosilylation reactions.[22,23] Silanization reactions involve first oxidising the freshly etched, hydride terminated surface to generate silanol groups, by means of an oxidising treatment.[24,25] These silanol groups can then react with alkoxy or chloro silane compounds to incorporate various chemical functionalities within the pores.[26,27] Compounds containing terminal functionality including amines, thiols and polyethylene glycol (PEG) can be incorporated via this method.[28–30] There are however limitations associated with silanization-based surface modification of pSi, most importantly the susceptibility for the Si–O–Si functionalized surface towards hydrolytic attack, causing the pSi structure to degrade.[31,32] Degradation may be desirable for specific applications including drug delivery and certain forms of biosensors, but the kinetics of degradation of silanized pSi surfaces can be prohibitive for other applications, in which case a more stable means of surface modification is required.[13,14]

Hydrosilylation reactions of freshly etched, hydride terminated pSi with alkene species are commonly used to produce more stable and robust surfaces.[33,34] These reactions involve the direct conjugation of an alkene (or alkyne) species to the Si–H surface, to form a stable Si-C bond.[35] This type of reaction can be used to incorporate a diverse range of chemical species, including carboxylic acids, thiols, esters, PEG and alcohols.[19,36–39] Hydrosilylation reactions are performed using a variety of methods, which include Lewis acid mediated and microwave assisted hydrosilylations.[40,41] Two popular methods for hydrosilylation reactions on pSi surfaces are thermal and light assisted hydrosilylations.[42,43] Precautions to eliminate

M. J. Sweetman, M. Ronci, S. R. Ghaemi, N. H. Voelcker
Flinders University
School of Chemical and Physical Sciences
GPO Box 2100, Adelaide, 5001, South Australia, Australia
E-mail: nico.voelcker@flinders.edu.au;
nico.voelcker@unisa.edu.au
J. E. Craig
Flinders University
Department of Ophthalmology
Bedford Park, Adelaide, 5042, South Australia, Australia

DOI: 10.1002/adfm.201102000

oxygen and water from hydrosilylation reactions are required, to prevent oxidation of the hydride terminated pSi surface, which can occur as a side reaction.[44,45]

Light assisted hydrosilylation reactions have been previously reported on flat silicon surfaces, however it was first reported on pSi surface by Stewart and Buriak, who demonstrated the conjugation of various alkene/yne species on the pSi structure.[46,47] They also highlighted the ability to selectively pattern the attachment of these compounds on pSi surfaces, by irradiating the surface through a photomask in the presence of an alkene species. Whilst the popularity of light assisted hydrosilylation reactions on both porous and flat silicon has grown in recent years,[48–52] no attempt has been made to take advantage of the ability to produce chemical patterns on pSi via this method.

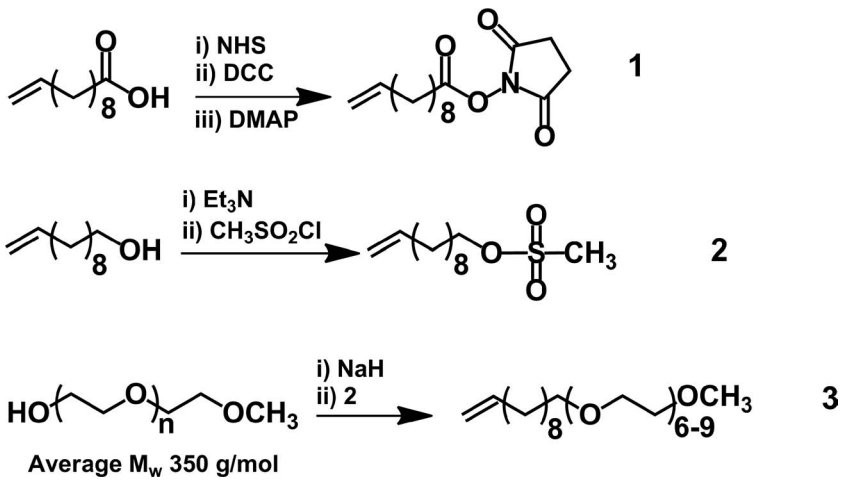

Figure 1. Schematic for the synthesis of NHS ester alkene **1**, intermediate mesylate functionalized alkene **2** and PEG functionalized alkene **3**.

Previous research into patterning pSi surfaces has focussed primarily on photolithography techniques (such as photoresist patterning and reactive ion etching) to form discrete etched regions on a silicon wafer.[53–55] Such pSi arrays have been used for biosensing and cell culture applications, as well as for producing surface-bound protein arrays.[56–60] Discrete, micron size arrays of pSi can be fabricated using such methods. Production of these pSi arrays is associated with disadvantages including the contamination of the surface with photoresist, the cumbersome nature of the procedure and the fact that this approach does not lead to a dual functionalized surface pattern. For applications in cell culture and biointerfaces, straightforward procedures to produce dual functionalized patterns on pSi would be highly desirable. We have recently demonstrated lateral patterning of dual chemical species across etched pSi surfaces, using a combination of photolithography and silanization techniques.[61] By this method, the guided attachment of mammalian cells to functionalized pSi surfaces was achieved. The use of pSi provides extra capabilities for cell scaffold and cell microarray applications. pSi is a biodegradable material, making it an excellent candidate for cell scaffold applications where cells can be initially positioned and cultured on the material and after some (controllable) time the pSi will dissolve leaving behind the desired cell/tissue matrix. In terms of cell microarrays, pSi allows not only the effect of surface-bound materials on cell to be investigated, but the internal porous area can also be loaded with different chemicals/biologicals giving rise to a platform where multiple factors can be investigated simultaneously. This may lead to high throughput screening platforms for different cell types. For both of these applications, the ability to discretely and selectively pattern chemical and biological materials on pSi surfaces is essential.

In this work, we describe lateral, dual surface functionalization of pSi with functional alkene species. UV light assisted hydrosilylation reaction with a pattern defined by a photomask and without the need for a photoresist is employed to attach the first alkene to the pSi surface. This is followed by a second UV initiated hydrosilylation with a different alkene in order to backfill the non-reacted surface sites. We used the dual surface functionalities for selective immobilization of patterned arrays of proteins on a single surface, which in turn provided the ability for the patterned attachment of mammalian cells. Functionalized pSi surfaces were characterized by IR microscopy, while protein arrays were characterized by MALDI MS imaging.

2. Results and Discussion

2.1. Synthesis of Functional Alkenes

The functional alkene compounds were synthesized as shown in **Figure 1**. The NHS functionalized alkene linker 1 was synthesized following a procedure adapted from Yin *et al.*[47] This alkene linker was employed to allow a one-step surface modification procedure, with the linker activated for immediate conjugation to an amine functional species.

Alkene 2 was synthesized as a precursor to the PEG functionalized alkene 3. In the case of alkene 2, undecylenyl alcohol was converted into a mesylate compound, which was immediately used for the synthesis of alkene 3. A short monomethyl PEG compound, with an average molecular weight of 350 g/mol was used to substitute the mesylate. As an average molecular weight PEG compound was used for the synthesis of alkene 3, the obtained crude product was purified by silica gel chromatography to separate the various length PEG alkene compounds from the starting material. The product after purification was alkene compounds containing six to nine ethylene glycol repeats. This product, of alkenes with mixed PEG lengths was used for all subsequent surface modification reactions. The surface modification procedure is depicted in the schematic in **Scheme 1** and is described in detail in the experimental methods.

2.2. Chemical Micropatterning by UV Hydrosilylation Using a Photomask

Functionalized pSi surfaces were characterized by IR spectroscopy and microscopy. **Figure 2** displays IR spectra from

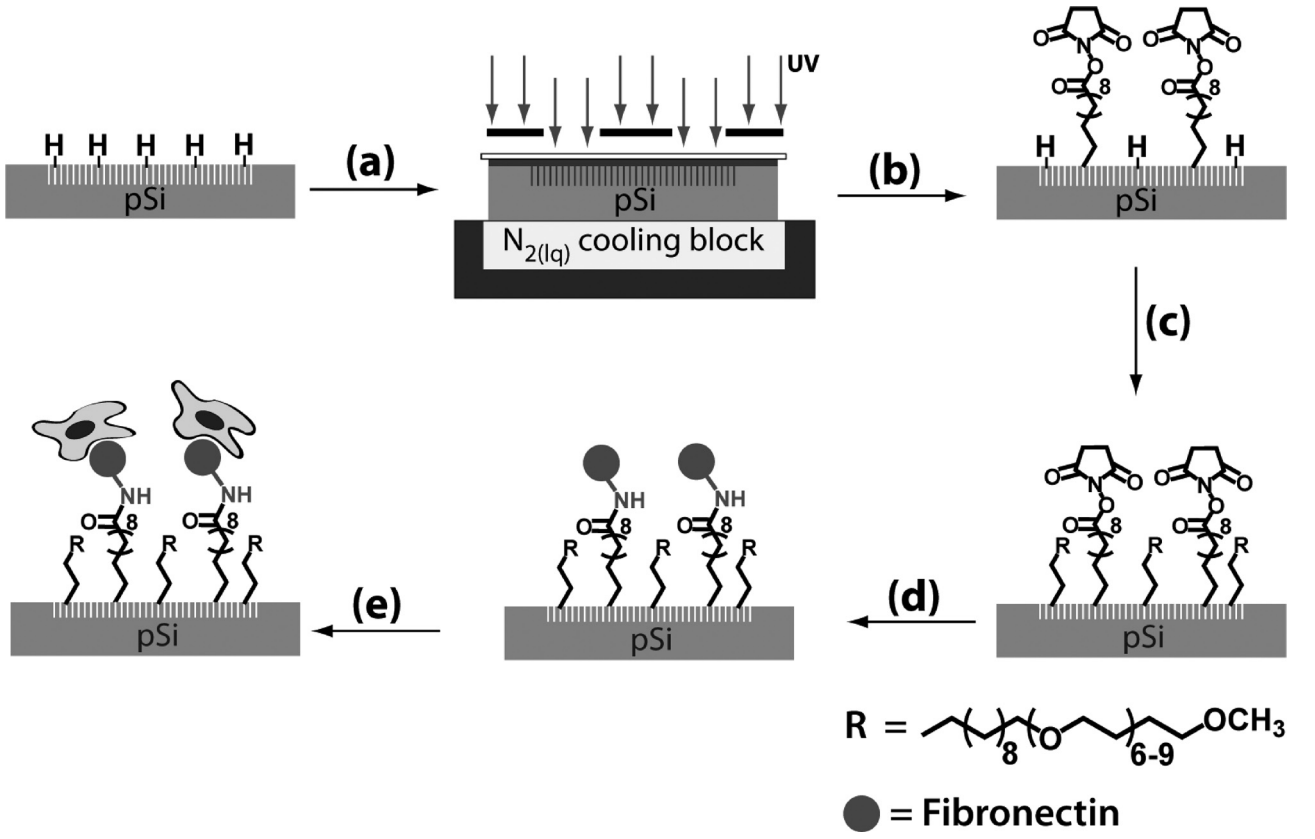

Scheme 1. Surface modification schematic, showing; a) UV initiated hydrosilylation using a photomask, b) washing of patterned porous surface, c) secondary hydrosilylation to backfill the remaining surface, d) FN conjugation to NHS ester functional groups, and finally, e) mammalian cell culture on FN patterned pSi surfaces.

pSi surfaces immediately after the UV hydrosilylation reaction using a photomask with the NHS alkene 1 (Figure 2a) and after both the patterning and secondary, backfill hydrosilylation reactions with the NHS and PEG alkenes, respectively (Figure 2b). Spectrum 1* in Figure 2a corresponds to an NHS alkene functionalized area on the surface. This spectrum shows low intensity peaks for methylene stretching vibrations at 2900 cm^{-1}, as well as a peak associated with the carbonyl stretching vibrations of the NHS ester at 1740 cm^{-1}.[62,63] These two peaks indicate the successful attachment of the NHS alkene linker in this region. Based on the intensity of the methylene and carbonyl peaks in spectrum 1* of Figure 2a, the coverage with the linker is well below a monolayer. The limited alkene coverage is due to the reaction conditions, where only a low alkene concentration (10 mM) and short reaction time (20 min) were used. Short reaction times were deliberately used to prevent non-specific reaction of the alkene in the non-irradiated areas which was a side reaction that became obvious for longer reaction times. Consistent with the limited alkene coverage, there is still a pronounced $Si–H_X$ vibrational peak at 2100 cm^{-1} in spectrum 1*.[31]

Spectrum 2* in Figure 2a corresponds to a masked area during the UV hydrosilylation reaction and displays a prominent $Si–H_X$ vibrational peak at 2100 cm^{-1}. There are no methylene or carbonyl vibrational peaks in spectrum 2*, showing that the NHS alkene has not reacted in this region on the surface. We observed that in addition to the short reaction times and low alkene concentration, cooling of the surface was essential to prevent hydrosilylation reaction from occurring outside of the regions exposed to UV light. We assumed that by cooling the surface, thermal reaction pathways were suppressed.

To stabilise the patterned pSi substrate, a second UV hydrosilylation reaction was performed, where the PEG alkene was incorporated into the surface. Following this second hydrosilylation, the pSi surface was again characterized by IR spectroscopy, with the spectrum obtained from a surface area encompassing both alkene functionalized regions. Figure 2b displays the IR spectrum for the patterned and stabilized surface, where there is a prominent methylene stretching vibration at 2900 cm^{-1}, as well as a terminal methyl stretching vibration at 1430 cm^{-1}.[64] Stretching vibrations at 1100 cm^{-1} correspond to Si–O bonds and indicate the presence of surface oxidation, a common side reaction in hydrosilylations of pSi.[63] There is also a carbonyl stretching vibrational peak at 1700 cm^{-1} corresponding to the carbonyl of the NHS ester functional groups present on the surface.[65] The $Si–H_X$ stretching vibrational peak at 2100 cm^{-1} is still present in the spectrum, indicating incomplete reaction of the alkene on the surface. This may be attributed to an impeded access of alkene to the reactive Si–H sites due to the steric bulk of the long PEG alkene species. This effect has been noted previously in hydrosilylation reactions.[45,66]

The pronounced methylene vibrational peaks in the spectrum in Figure 2b suggest the incorporation of a large amount

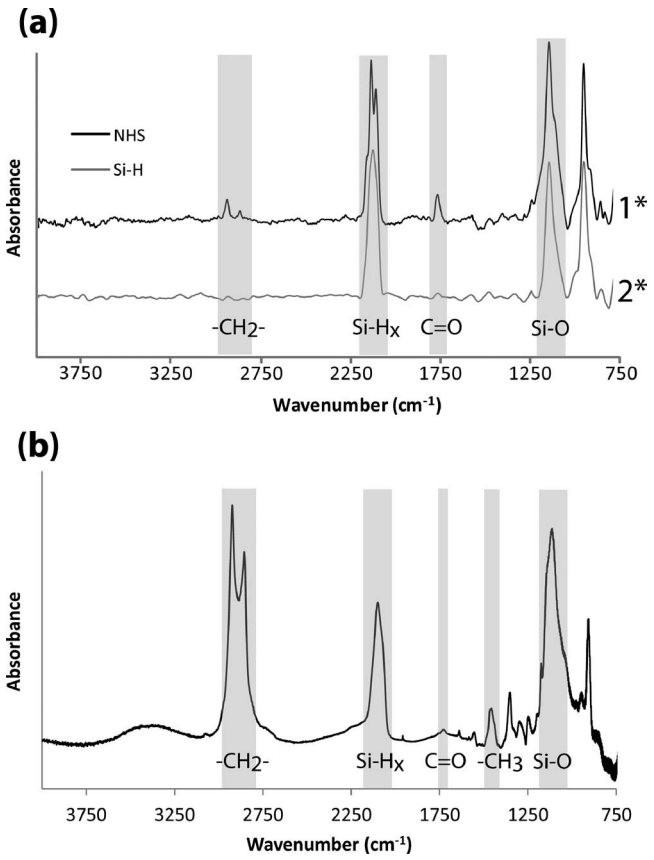

Figure 2. a) IR spectra from an NHS alkene patterned pSi surface, with spectrum 1* obtained from within a patterned region and spectrum 2* obtained from the surrounding Si–H terminated pSi surface area. 1* and 2* correspond to the labelled areas in Figure 3a. b) Displays an IR spectrum of a pSi surface after both the UV initiated hydrosilylation with a photomask and the secondary backfill hydrosilylation reaction without a mask.

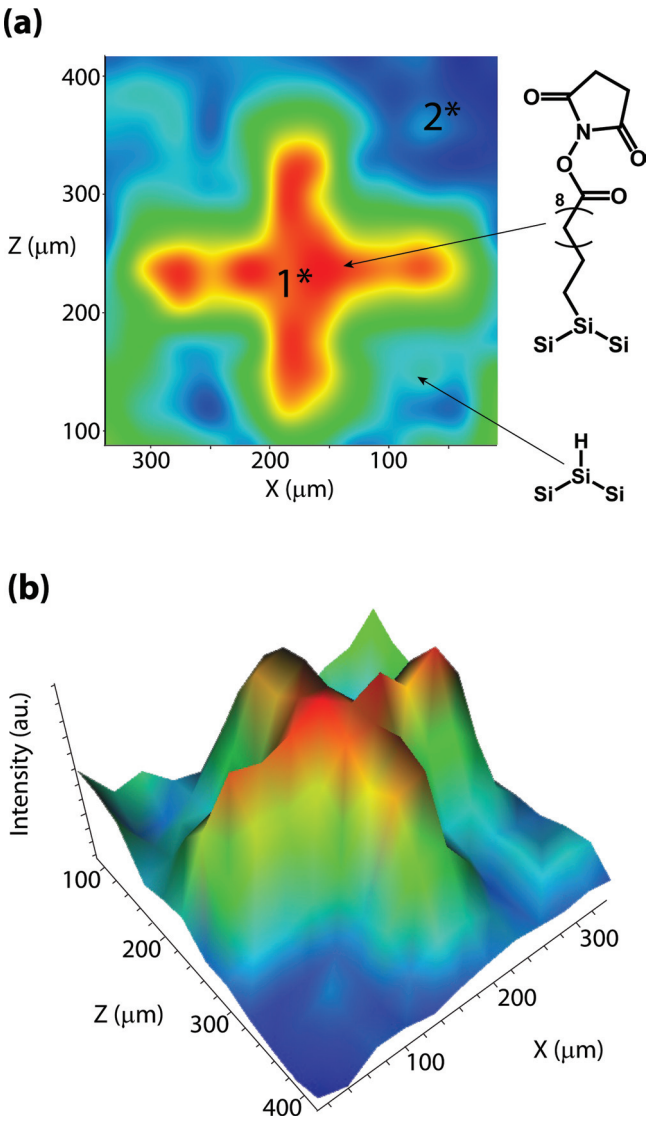

Figure 3. a) 2D IR microscopy map of NHS alkene patterned pSi surface, displaying a cross feature. The map has been produced from the intensity of the integrated carbonyl peak at 1700 cm^{-1}, associated with the NHS ester. 1* and 2* indicate the positions from where the corresponding IR spectra in Figure 2a are acquired from, with the surface chemistry in each of these regions also displayed. b) Displays a 3D representation of the IR map.

of the alkene species and hence Si−C bonds that increase the stability of the functionalized pSi surface. A degradation profile of the dual hydrosilylation functionalized surface and of the single hydrosilylation photopatterned surface was recorded as a measure of overall surface stability, (see supporting information, Figure S1). The two degradation profiles display the change in effective optical thickness (EOT) of the two pSi films over time, in PBS. A steeper negative slope in the degradation profile corresponds to lower surface stability and hence an increased rate of surface dissolution/degradation in the aqueous media.[34] While the single hydrosilylation photopatterned surface showed a rapid degradation, due to the high level of unstable Si–H bonds on the surface (Figure 2a, Spectrum 1*), the dual hydrosilylation functionalized surface showed only a 0.6% change in EOT after 2 h in aqueous media, indicating a highly stable surface.[32]

IR microscopy was also used to characterise the patterned pSi surfaces, with **Figure 3** displaying a 2D and 3D IR map of a cross-shaped feature. These IR maps were obtained immediately after the initial UV hydrosilylation reaction using the photomask. The 2D and 3D plots in Figure 3a and Figure 3b display an intensity map of the carbonyl stretching vibrational peak associated with the NHS ester functional group. It can be seen that the carbonyl stretching vibrational intensity is fairly homogeneously distributed across the patterned feature, and drops sharply at the edges (Figure 3b). These IR maps confirm that the NHS alkene has only been conjugated to the surface within the patterned features. Figure 3a indicates the positions (1* and 2*) from where the IR spectra in Figure 2a were obtained, along with a schematic showing the respective surface chemistry.

Fluorescent organic dyes were also used to confirm chemical patterning on the functionalized pSi surfaces, with the amine functionalized dye lissamine, conjugated to the NHS ester

of a pSi surface patterned with the NHS-functionalized alkene 1 and stabilized with PEG alkene 3. Figure S2 in the Supporting Information shows excellent confinement of the immobilized dye to the patterns defined by the features on the photomask. There are very low levels of background fluorescence in the images, which indicates there were very low levels of cross-reaction of NHS ester alkene within the non-illuminated areas of the pSi surface during the UV hydrosilylation reaction.

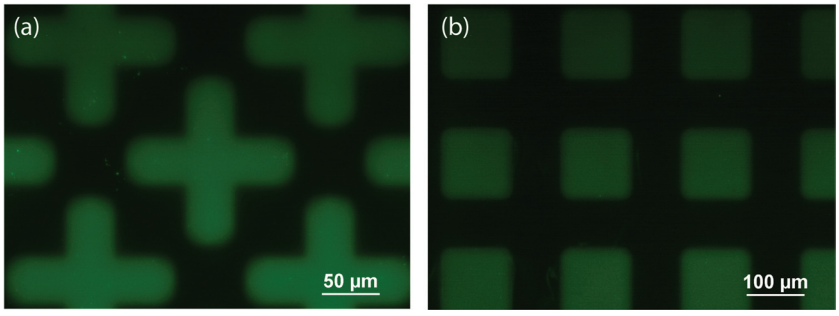

Figure 4. Fluorescence microscopy images showing patterns of FITC-BSA immobilized onto NHS ester, alkene 1 patterned pSi surfaces with PEG alkene 3 attached in the surrounding areas.

2.3. Conjugation of Proteins to Micropatterned pSi Films

Functional surfaces for life science applications benefit from the ability to immobilise specific biological factors such as proteins or DNA. At the same time, it is often required that these surfaces prevent the non-specific adsorption of unwanted biological factors or cell attachment. The most common chemical functionality for preventing the non-specific adsorption of biological species to surface is PEG.[67,68] The two requirements both apply in the field of cell microarrays where proteins or other biological factors are presented in an array format.[69] Cells are then seeded on the factors displayed on the surface and cell attachment to the areas not displaying biological factors is not desired. It would therefore be advantageous if specific biological factors could be immobilized in patterned regions on a functionalized pSi surface, while the remaining surface would prevent the adsorption of unwanted species. This concept was pursued using the presented patterning technique for pSi surfaces.

To initially demonstrate the ability to produce patterns of immobilized proteins, the 'sticky' protein bovine serum albumin (BSA) was incubated with a chemically patterned pSi surface. The NHS ester of alkene 1 would allow covalent immobilization of BSA whilst the PEG tether of alkene 3 was meant to prevent non-specific protein adsorption. Fluorescein isothiocyanate modified BSA (FITC-BSA) was used to visualise the protein attachment to the patterned surface. **Figure 4** displays the observed fluorescence microscopy images, demonstrating that the FITC-BSA is indeed confined to the crosses or squares functionalized with alkene 1, with a low fluorescence signal observed in the areas outside of the patterns, which are functionalized with alkene 3. This confirms that there is little to no non-specific adsorption of the FITC-BSA to the PEG functionalized areas on the pSi surface.

For patterned pSi surfaces to be used for cell culture applications, the cell adhesion mediator protein fibronectin (FN) was conjugated to chemically patterned pSi, in the same manner as the FITC-BSA. In this case the protein (FN) was not fluorescently labelled and MALDI MS imaging was instead used to map protein distribution on the functionalized pSi surface. In order to confirm the presence of FN bound selectively inside the pattern, the surface was covered with a spray of finely dispersed trypsin droplets via a piezoelectric automatic sprayer, generating FN-derived peptides used to produce peptide mass fingerprints (PMF). The surface was subsequently covered with MALDI matrix and analysed. Together with the MALDI MS imaging run a spectrum in reflectron positive (RP) mode was also recorded and used for the protein database search. The search confirmed the presence of FN with a score of 152. The signal of one representative tryptic peptide was chosen to produce the ion intensity map which revealed the patterned distribution of FN.

Figure 5a displays a representative MALDI RP spectrum, acquired from within a patterned region on the surface (after trypsin digestion). Figure 5b shows the virtual ion intensity

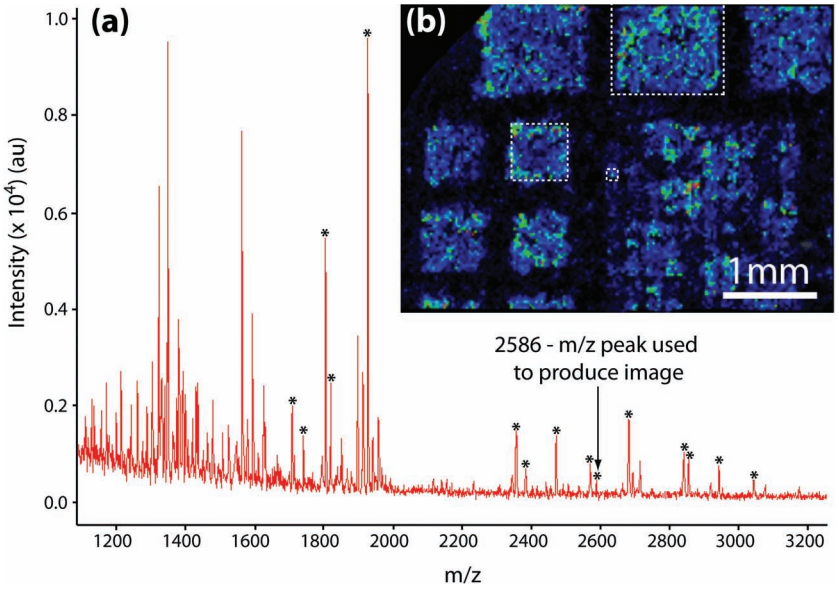

Figure 5. a) MALDI mass spectrum in reflectron positive mode acquired within the pattern after trypsin digestion and b) virtual image showing the distribution of the signal at m/z = 2586 (arrow), derived from FN conjugated to functionalized pSi. The peaks marked with an asterisk represent those matched with the theoretical tryptic digest of FN. The dashed outlines in (b) indicate the expected patterned areas of FN attachment.

map of the FN conjugated pSi surface. The signal corresponding to the peptide at m/z = 2586 was used to produce the ion intensity map. It can be seen that this tryptic peptide, derived from FN, is concentrated within the square pattern regions. The large and medium squares (1 mm^2 and 0.5 mm^2) display the best resolution of the patterned FN, while the array of smaller squares (100 μm^2) is beyond the spatial resolution limit of the instrument. As the surface bound protein was digested with trypsin in the liquid phase, some amount of diffusion of the peptide fragments outside of the patterned regions, across the surface may have occurred.

Figure 5b demonstrates that the FN has been successfully conjugated to the pSi surface within the patterned features, where the NHS alkene 1 is located. Furthermore, the PEG alkene 3 successfully prevents the non-specific adsorption of the FN in the areas surrounding the patterns, in the same manner as for FITC-BSA surface conjugation.

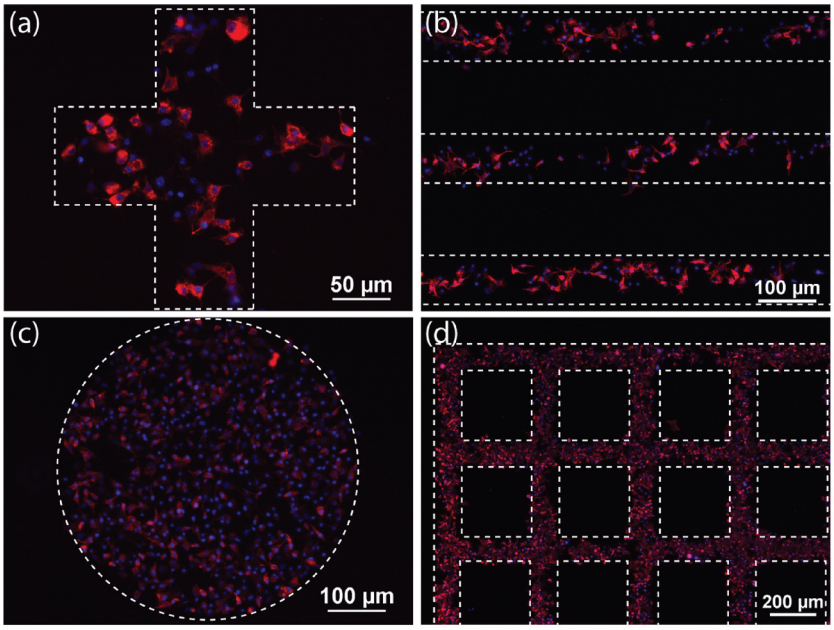

Figure 6. SK-N-SH cell attachment to functionalized pSi surfaces displaying patterned arrays of FN, surrounded by PEG functionality. a) Displaying a cross shaped pattern, b) horizontal lines, c) showing a circular shaped pattern and (d) a grid where the inner squares display PEG functionality. Cells are stained with Hoechst and phalloidin (tertamethylrhodamine B conjugated). The dashed lines provide a visual reference for the patterned areas (i.e., areas displaying FN) on the pSi surfaces.

2.4. Micropatterning of Neuroblastoma Cells on pSi

Following the attachment of proteins on chemically micropatterned pSi, the interaction and patterned attachment of the human neuroblastoma cell line SK-N-SH was investigated. For this investigation, the extracellular matrix protein FN was first immobilized in the patterned regions, in the same manner as previously described. FN was chosen to investigate cell patterning because of its ability to mediate cell adhesion to surfaces, through interaction with integrins on the cell membrane.[70] FN has previously been demonstrated to promote cell attachment to homogeneous surfaces and facilitate patterned cell attachment to surfaces displaying arrays of the protein.[34,71]

FN was conjugated to functionalized pSi surfaces, displaying the NHS alkene 1 in the patterned regions, with the PEG alkene 3 in the surrounding areas. SK-N-SH cells were then cultured on these functionalized surfaces. **Figure 6** displays fluorescence microscopy images of the cells attached to the patterned surfaces, after Hoechst and phalloidin (tetramethylrhodamine B conjugated) staining. The patterned areas of the surface where the FN has been attached are outlined in the figure as a guide to the eye. Figure 6a,b,c display a cross shape, horizontal lines and a circular shape respectively, with FN immobilized inside each of the patterned areas, while Figure 6d displays a grid pattern where the grid has been functionalized with FN and the squares display PEG. It can be seen that more than 99% of all cells on the surface attached within the fibronectin-functionalized regions. The images also demonstrate the versatility of this surface patterning technique in terms of possible sizes and shapes of the patterned features in comparison to traditional microprinting techniques.[72]

Phalloidin staining of the actin filaments of the cell cytoskeleton was used to characterise the cell attachment and in particular assess cell spreading on the functionalized surfaces. The SK-N-SH cells are attaching to the pSi surface through interaction of the FN with cell membrane bound integrins with Figure 6a,b showing that the cells have begun to spread on the surface even after a timeframe of 6 h.

It should be noted that the size of the cell patterns displayed in Figure 6 are smaller than the FN patterns resolved by MALDI MS imaging. This suggests that although the MALDI MS imaging could not resolve surface patterned featured below approximately 500 μm^2, it was still possible to produce FN patterns with feature sizes smaller than this.

3. Conclusion

We describe the synthesis and patterned attachment of different alkene species to pSi surfaces, through UV initiated hydrosilylation reactions using a photomask. Photopatterned attachment of an NHS ester functionalized alkene species followed by a second hydrosilylation reaction to backfill the rest of the surface with a second alkene, afforded stable and chemically patterned pSi surfaces.

The patterned attachment of biological species to functionalized pSi surfaces was also demonstrated through the conjugation of FITC-BSA to a surface displaying patterned areas of NHS ester alkene, surrounded by a PEG functionalized alkene. pSi surfaces patterned with the cell adhesion mediator protein FN were also produced, as confirmed by MALDI MS imaging.

The FN functionalized pSi surfaces were shown to successfully guide the surface attachment of the mammalian neuroblastoma cell line SK-N-SH, with greater that 99% of cells attaching in the patterned regions.

The biocompatible nature of pSi and the relative ease and versatility of the described photoresist-free patterning technique make this surface modification procedure highly applicable to a range of biomaterial applications. The technique is compatible with surface conjugation of a wide range of biological species. Chemically and biologically patterned pSi surfaces may find application as cell microarrays and degradable tissue culture substrates or as in in vitro cell culture systems, where the porous material is used to deliver bioactive compounds to cells. Specialized biosensors may also be developed using these substrates. The described patterning technique allows high levels of control over feature size and shape, with cell attachment to patterned areas smaller than those for conventional microarrays possible.

4. Experimental Section

Chemicals: Chemicals used for organic synthesis and surface modification were purchased from Sigma-Aldrich (USA), unless stated otherwise. All organic solvents were distilled prior to use, following standard laboratory procedure.[73]

Organic Synthesis: Synthesis of undec-10-enoic acid 2,5-dioxo-pyrrolidin-1-yl ester **1**: A mixture of *N,N′*-dicyclohexylcarbodiimide (DCC) (6.15 g, 29.81 mmol) and 4-dimethylaminopyridine (DMAP) (0.33 g, 2.71 mmol) in dimethylformamide (DMF) (10 mL) was added dropwise to a stirred solution of undecylenic acid (5.00 g, 27.1 mmol) and NHS (3.12 g, 27.1 mmol) in DMF (40 mL) at 0 °C. The solution was allowed to warm to room temperature and was stirred for a further 24 h. After completion of the reaction, the solution was cooled to 0 °C and passed through a sintered glass filter. The filtrate was washed with DCM (50 mL) and the solvents were combined and removed under vacuum. The crude product was purified by silica gel column chromatography (100% DCM). Similar fractions were combined and concentrated by rotary evaporation, yielding the pure product as a white solid, designated **1** (6.5 g, 85%). ^{1}H NMR (400 MHz, $CDCl_3$) δ 5.88–5.74 (m, 1H), 5.03–4.92 (m, 2H), 2.8 (s, 4H), 2.6 (t, J = 7.5 Hz, 2H), 2.05 (q, J = 7 Hz, 2H), 1.75 (qui, J = 7 Hz, 2H), 1.31 (m, 10H).

Synthesis of Methanesulfonic Acid undec-10-enyl ester **2**: Triethylamine (13.2 mL, 94.7 mmol) was added to a solution of undecylenyl alcohol (12.0 mL, 59.6 mmol) in DCM (250 mL) under inert atmosphere (nitrogen), with stirring at 0 °C. Methanesulfonyl chloride (6.1 mL, 66.3 mmol) was then added dropwise over a period of 5 min with stirring. Stirring for an additional 24 h allowed for completion of the reaction. The reaction mixture was transferred to a separating funnel and washed with ice water (2 × 100 mL), followed by 10% HCl solution (2 × 100 mL), saturated sodium bicarbonate solution (2 × 100 mL) and brine (2 × 100 mL). The organic phase was subsequently dried over $MgSO_4$ and concentrated by rotary evaporation to give a yellow oil, methanesulfonic acid undec-10-enyl ester, designated **2** (13.87 g, 94%). ^{1}H NMR (400 MHz, $CDCl_3$) δ 5.86–5.73 (m, 1H), 5.00–4.90 (m, 2H), 4.20 (t, J = 6.6 Hz, 2H), 2.99 (s, 3H), 2.03 (q, J = 6.6 Hz, 2H), 1.73 (qui, J = 6.6 Hz, 2H), 1.272 (m, 12H).

Synthesis of Undec-10-enyl-oligoethylene glycol **3**: Polyethylene glycol monomethyl ether (Av. M_w 350 g mol^{-1}) (23.4 g, 66.7 mmol) was added dropwise to a stirred solution of NaH (2.7 g of a 60% suspension in oil, 66.7 mmol) in THF (100 mL) on ice, under nitrogen. After addition of all of the polyethylene glycol monomethyl ether the mixture was stirred at room temperature for a further 2 h. After this time, **2** (13.9 g, 55.8 mmol) was slowly added to the solution over a period of 30 min and the solution was stirred at room temperature for a further 48 h to allow completion of the reaction. The reaction was quenched with ice water (50 mL) and the organic product was extracted with diethyl ether (2 × 100 mL). The organic phase was collected and washed with cold brine (2 × 50 mL) and water (2 × 50 mL) and concentrated by rotary evaporation to give a pale yellow oil. The crude product was purified by silica gel column chromatography (100% diethyl ether), to remove any starting material, with similar fractions combined and concentrated by rotary evaporation. The major products were alkene compounds containing six to nine ethylene glycol repeats (16.08 g, 76%), with NMR reported for the obtained alkenes (designated **3**). ^{1}H NMR (400 MHz, $CDCl_3$) δ 5.88–5.74 (m, 1H), 5.02–4.91 (m, 2H), 3.71–3.63 (m, 24H), 3.59–3.55 (m, 4H), 3.45 (t, J = 6.9 Hz, 2H), 3.38 (s, 3H), 2.05 (q, J = 6.9 Hz, 2H), 1.58 (qui, J = 6.6, 2H), 1.28 (m, 12H).

pSi Preparation: P-type silicon wafers (<1 μΩ.cm, Siltronix, France) were rinsed with methanol (Chem Supply, Australia), acetone (Ajax Finechem, USA) and DCM (Biolab, Australia), before being clamped into a Teflon etching cell. The silicon wafer was then etched using a 2425 Source Meter (Keithley, USA) as the current source. The wafers were etched using the following conditions: etching solution 3:1 HF (48% aqueous) (Merck, Germany)/EtOH (Merck, Germany), etching time 300 s, etching current 20 mA cm^{-2}. After etching, the HF was removed and the surface was washed with methanol, acetone and DCM and dried under a gentle stream of nitrogen.

UV Initiated Hydrosilylation Using a Photomask: The preparation of chemically patterned pSi surfaces is depicted in Scheme 1, with the experimental procedure performed as follows. A freshly etched pSi sample was wetted with a solution of alkene 1 (10 mM) in toluene and a glass coverslip was placed over the sample to retain the solution within the pores and prevent solvent evaporation. This sample was then placed onto a cooling block (cooled by liquid nitrogen) and a photomask (Bandwidth Foundry, Australia) displaying arrays of circles, squares, lines, crosses and grids with feature dimensions of 20–500 μm, was placed directly onto the pSi surface. The sample was irradiated for 20 min using an Omnicure S1000 (EXFO Life Sciences and Industrial Division, Canada) UV light source of 100 W intensity, at a distance of 2 cm, Scheme 1a. After irradiation, the coverslip was removed and the pSi sample was washed with ethanol and acetone and dried under a stream of nitrogen, Scheme 1b.

Secondary Hydrosilylation on Photopatterned pSi: Immediately following the first UV initiated hydrosilylation reaction, pSi surfaces were subject to a second hydrosilylation reaction with alkene 3, Scheme 1c. For alkene 3, the pSi surface was clamped into a Teflon reaction cell and covered with neat alkene 3. The pSi surface was then irradiated by UV light of 100 W intensity, at a distance of 2 cm for 2 h. Following UV irradiation the surface was washed with copious amounts of ethanol and dried under a gentle stream of nitrogen.

Protein Conjugation: An alkene 1 and 3 functionalized pSi surface was reacted with a solution of FITC-BSA or FN (500 μg mL^{-1}) in PBS at pH 7.4. The surface was allowed to react for 3 h in the protein solution, after which it was removed from the reaction cell and washed with PBS-Tween (0.5%), PBS and MilliQ H_2O and dried under a stream of nitrogen, Scheme 1d. Surfaces functionalized with FN were stored at 4 °C in the dark for up to one week, prior to use in cell culture experiments.

Cell Culture: SK-N-SH human neuroblastoma cells were cultured in Dulbecco's Modified Eagle Medium (DMEM) (JRH Bioscience, USA) containing 5 mM L-glutamine, 100 IU mL^{-1} penicillin, 100 μg mL^{-1} streptomycin sulphate (Invitrogen, USA) and 10% v/v fetal bovine serum (FBS) (Bovogen Biologicals, Australia) and maintained at 37 °C in 5% CO_2. To investigate cell attachment to the biologically functionalized surfaces, cells were incubated in contact with the surfaces at a density of 2.6 × 10^6 cells mL^{-1} and cultured for 6 h in DMEM containing 5 mM L-glutamine, 100 IU mL^{-1} penicillin, 100 μg mL^{-1} streptomycin sulphate and 10% v/v FBS and maintained at 37 °C in 5% CO_2, Scheme 1e. During the final 30 min of the incubation period, Hoechst 33342 (Molecular Probes, USA) was added to the culture solution for each surface to a final concentration of 2 μg mL^{-1}. Following Hoechst staining, each surface was rinsed with PBS (pH 7.4) and PBS-Tween (0.5%) to remove any non-specifically or weakly attached cells. Cells were then fixed with

4% w/v paraformaldehyde (Electron Microscopy Sciences, Australia) in PBS for 10 min, washed with PBS and permeabilized with 0.1% Triton-X100 in PBS for 5 min. Finally, cells were stained with 0.38 μM phalloidin (tetramethylrhodamine B isothiocyanate conjugated) solution (300 μL) in PBS for 30 min in the dark and then washed with PBS. Each surface was mounted on a glass slide, covered with gel mount media and a coverslip.

Fluorescence Microscopy: Fluorescence microscopy was performed on an Eclipse 50i microscope equipped with a D-FL universal epi-fluorescence attachment and a 100 W mercury lamp (Nikon Instruments, Japan). Fluorescence images were captured with a CCD camera (Nikon Instruments, Japan), using the following fluorescent filters ex. 385-400/em. 450-465 nm, ex. 545-565/em. 580-620 nm. Images were analysed using NIS-elements v3.07 software (Nikon Instruments, Japan).

IR Spectroscopy and Microscopy: IR spectroscopy and microscopy were performed on a Nicolet iN10 infrared microscope (Thermo Electron Corporation, USA). IR spectroscopy was collected in ATR mode using a Germanium ATR crystal and a cooled MCT detector. IR spectra were captured using an aperture size of 150 μm^2 and were recorded over a range of 675–4000 cm^{-1}, at a resolution of 8 cm^{-1} and taken as an average of 64 scans. A spectrum of ambient air was used as a background. IR microscopy data was collected using transmission mode with a cooled MCT detector. IR spectra were captured using an aperture size of 30 μm^2 and were recorded over a range of 675–4000 cm^{-1}, at a resolution of 8 cm^{-1} and taken as an average of 64 scans. An air background was used as a blank for all spectra collected. Analysis of IR microscopy data was performed using OMNIC Picta software (Thermo Electron Corporation, USA).

MALDI MS Imaging - Sample Preparation: 200 μL of a 0.1 mg mL^{-1} trypsin solution in 10 mM $(NH_4)HCO_3$) was deposited in several cycles using an ImagePrep (Bruker-Daltonics) piezoelectric automatic sprayer at room temperature, allowing the samples to partially dry between each cycle. After trypsin deposition, digestion was carried out for 1 h. The samples were then coated with a solution of 7 mg mL^{-1} CHCA in TFA 0.2%/ACN 50:50 using the ImagePrep piezoelectric automatic sprayer. *Image acquisition:* MALDI imaging was performed according to the procedure described by Ronci et al. on a Bruker Autoflex III MALDI MS/MS (Bruker, Germany).[74] Mass spectrometric imaging analysis was performed in linear positive mode in the range 1–10 kDa with a spatial resolution of 100 μm. Fleximaging 2.1 (build 25) (Bruker-Daltonics) was used to control Flexcontrol 3.3 (build 85) during the acquisition. Fleximaging was used to extract the ion intensity map images, after processing the datasets by baseline subtraction, normalization and data reduction. ClinProTools 2.2 (build 83) was used as spectra class analysis and visualization tool.

Supporting Information

Supporting Information, including pSi surface stability and fluorescent dye conjugation procedures and figures, is available from the Wiley Online Library or from the author.

Acknowledgements

Flinders University and the Australian Research Council are kindly acknowledged for financial support.

Received: August 24, 2011
Published online: January 19, 2012

[1] B. Sciacca, F. Frascella, A. Venturello, P. Rivolob, E. Descrovi, F. Giorgis, F. Geobaldo, *Sens. Actuators, B* **2009**, *137*, 467–470.
[2] V. S. Y. Lin, K. Motesharei, K. S. Dancil, M. J. Sailorand, M. R. Ghadiri, *Science* **1997**, *278*, 840–843.
[3] V. Chin, B. E. Collins, M. J. Sailor, S. N. Bhatia, *Adv. Mater.* **2001**, *13*, 1877–1880.
[4] E. J. Anglin, M. P. Schwartz, V. P. Ng, L. A. Perelman, M. J. Sailor, *Langmuir* **2004**, *20*, 11264–11269.
[5] J. Torres, H. M. Martinez, J. E. Alfonso, L. D. Lopez, *Microelectron. J.* **2008**, *39*, 482–484.
[6] J. Gao, Y. Gao, Y. Y. Li, M. J. Sailor, *Langmuir* **2002**, *18*, 2229–2233.
[7] A. Jane, R. Dronov, A. Hodges, N. H. Voelcker, *Trends Biotechnol.* **2009**, *27*, 230–239.
[8] S. P. Low, K. A. Williams, L. T. Canham, N. H. Voelcker, *Biomaterials* **2006**, *27*, 4538–4546.
[9] L. T. Canham, in *Properties of Porous Silicon* (Eds. Institution of Engineering and Technology, London **1997**, pp. 416.
[10] J. Park, L. Gu, G. von Maltzahn, E. Ruoslahti, S. N. Bhatia, M. J. Sailor, *Nat. Mater.* **2009**, *8*, 331–336.
[11] A. H. Mayne, S. C. Bayliss, P. Barr, M. Tobin, L. D. Buckberry, *Phys. Stat. Sol. A* **2000**, *182*, 505–515.
[12] S. P. Low, N. H. Voelcker, L. T. Canham, K. A. Williams, *Biomaterials* **2009**, *30*, 2873–2880.
[13] N. H. Voelcker, I. Alfonso, M. R. Ghadiri, *ChemBioChem* **2008**, *9*, 1776–1786.
[14] A. O. Jane, E. J. Szili, J. H. Reed, T. P. Gordon, N. H. Voelcker, in *BioMEMS and Nanotechnology III* (Eds. SPIE, **2008**, 679908/1–679908/11.
[15] K. A. Kilian, L. M. H. Lai, A. Magenau, S. Cartland, T. Bocking, N. Di Girolamo, M. Gal, K. Gaus, J. J. Gooding, *Nano Lett.* **2009**, *9*, 2021–2025.
[16] M. P. Schwartz, A. M. Derfus, S. D. Alvarez, S. N. Bhatia, M. J. Sailor, *Langmuir* **2006**, *22*, 7084–7090.
[17] S. Ciampi, J. B. Harper, J. J. Gooding, *Chem. Soc. Rev.* **2010**, *39*, 2158–2183.
[18] H. L. Li, A. P. Fu, D. S. Xu, G. L. Guo, L. L. Gui, Y. Q. Tang, *Langmuir* **2002**, *18*, 3198–3202.
[19] J. T. C. Wojtyk, K. A. Morin, R. Boukherroub, D. D. M. Wayner, *Langmuir* **2002**, *18*, 6081–6087.
[20] J. Salonen, E. Laine, L. Niinisto, *J. Appl. Phys.* **2002**, *91*, 456–561.
[21] B. Sciacca, S. D. Alvarez, F. Geobaldo, M. J. Sailor, *Dalton Trans.* **2010**, *39*, 10847–10853.
[22] J. M. Buriak, *Adv. Mater.* **1999**, *11*, 265–267.
[23] M. P. Schwartz, F. Cunin, R. W. Cheung, M. J. Sailor, *Phys. Stat. Sol. A* **2005**, *202*, 1380–1384.
[24] J. Salonen, V. P. Lehto, E. Laine, *Appl. Phys. Lett.* **1996**, *70*, 637–639.
[25] S. Y. Chena, Y. H. Huangb, H. K. Laia, C. Lia, J. Y. Wanga, *Solid State Commun.* **2007**, *142*, 358–362.
[26] M. J. Sailor, E. J. Lee, *Adv. Mater.* **1997**, *9*, 783–793.
[27] M. P. Stewart, J. M. Buriak, *Adv. Mater.* **2000**, *12*, 859–869.
[28] B. Xia, L. Jun, X. Shou-Jun, G. Dong-Jie, W. Jing, P. Yi, Y. Xiao-Zeng, *Chem. Lett.* **2005**, *34*, 226–227.
[29] R. Yamaguchi, K. Miyamoto, K. Ishibashi, A. Hirano, S. M. Said, Y. Kimura, M. Niwano, *J. Appl. Phys.* **2007**, *102*, 014303-1–014303-7.
[30] Y. L. Khung, S. D. Graney, N. H. Voelcker, *Biotechnol. Prog.* **2006**, *22*, 1388–1393.
[31] I. N. Lees, H. Lin, C. A. Canaria, C. Gurtner, M. J. Sailor, G. M. Miskelly, *Langmuir* **2003**, *19*, 9812–9817.
[32] D. Xu, L. Sun, H. Li, L. Zhang, G. Guo, X. Zhao, L. Gui, *New J. Chem.* **2002**, *27*, 300–306.
[33] K. S. Dancil, D. P. Greiner, M. J. Sailor, *J. Am. Chem. Soc.* **1999**, *121*, 7925–7930.
[34] M. J. Sweetman, F. J. Harding, S. D. Graney, N. H. Voelcker, *Appl. Surf. Sci.* **2011**, *257*, 6768–6774.
[35] M. P. Stewart, E. G. Robins, T. W. Geders, M. J. Allen, H. Cheul Choi, J. M. Buriak, *Phys. Stat. Sol. (a)* **2000**, *182*, 109–115.
[36] M. J. Sweetman, S. D. Graney, N. H. Voelcker, in *BioMEMS and Nanotechnology III* (Eds. SPIE, **2008**, 679907/1–679907/12.
[37] K. A. Kilian, T. Bocking, K. Gausc, M. Galb, J. J. Gooding, *Biomaterials* **2007**, *28*, 3055–3062.
[38] R. Boukherroub, D. D. M. Wayner, D. J. Lockwood, J. T. C. Wojtyk, *J. Electrochem. Soc.* **2002**, *149*, H59–H63.

[39] B. Sweryda-Krawiec, T. Cassagneau, J. H. Fendler, *J. Phys. Chem. B* **1999**, *103*, 9524–9529.
[40] J. M. Buriak, M. P. Stewart, T. W. Geders, M. J. Allen, H. Cheul Choi, J. Smith, D. Raftery, L. T. Canham, *J. Am. Chem. Soc.* **1999**, *121*, 11491–11502.
[41] R. Boukherroub, A. Petit, A. Loupy, J. N. Chazalviel, F. Ozanam, *J. Phys. Chem. B* **2003**, *107*, 13459–13462.
[42] S. Ciampi, T. Böcking, K. A. Kilian, J. B. Harper, J. J. Gooding, *Langmuir* **2008**, *24*, 5888–5892.
[43] M. P. Stewart, J. M. Buriak, *J. Am. Chem. Soc.* **2001**, *123*, 7821–7830.
[44] L. Scheres, M. Giesbers, H. Zuilhof, *Langmuir* **2010**, *26*, 4790–4795.
[45] T. Bocking, K. A. Kilian, K. Gaus, J. J. Gooding, *Adv. Func. Mater.* **2008**, *18*, 3827–3833.
[46] M. P. Stewart, J. M. Buriak, *Angew. Chem. Int. Ed.* **1998**, *37*, 3257–3260.
[47] H. B. Yin, T. Brown, R. Greef, J. S. Wilkinson, T. Melvin, *Microelectron. Eng.* **2004**, *73–74*, 830–836.
[48] Q. Y. Sun, L. C. P. M. de Smet, B. van Lagen, M. Giesbers, P. C. Thune, J. van Engelenburg, F. A. de Wolf, H. Zuilhof, E. J. R. Sudholter, *J. Am. Chem. Soc.* **2005**, *127*, 2514–2523.
[49] T. Bocking, M. James, H. G. L. Coster, T. C. Chilcott, K. D. Barrow, *Langmuir* **2004**, *20*, 9227–9235.
[50] E. Fanizza, P. D. Cozzoli, M. L. Curri, M. Striccoli, E. Sardella, A. Agostiano, *Adv. Func. Mater.* **2007**, *17*, 201–211.
[51] S. Singh, S. N. Sharma, Govind, M. A. Khan, P. K. Singh, in *Transport Opt. Properties Nanomater.* (Eds: P. K. Singh, R.H. Lipson) AIP, Allahad, India, **2009**, 421.
[52] J. Nelles, D. Sendor, A. Ebbers, F. M. Petrat, H. Wiggers, C. Schulz, U. Simon, *Colloid Polym. Sci.* **2007**, *285*, 729–736.
[53] M. Kruger, R. Arens-Fischer, M. Thonissen, H. Munder, M. G. Berger, H. Luth, S. Hilbrich, W. Theiss, *Thin Solid Films* **1996**, *276*, 257–260.
[54] M. Ohmukai, K. Okada, Y. Tsutsumi, *J. Mater. Sci.: Mater. Electron.* **2005**, *16*, 119–121.
[55] V. V. Starkov, E. Y. Gavrilin, J. Konle, H. Presting, A. F. Vyatkin, U. König, *Phys. Stat. Sol. A* **2003**, *197*, 150–157.
[56] I. Rea, A. Lamberti, I. Rendina, G. Coppola, M. Gioffrè, M. Iodice, M. Casalino, E. De Tommasi, L. De Stefano, *J. Appl. Phys.* **2010**, *107*, 014513-1– 014513-4.
[57] H. F. Li, H. M. Han, Y. G. Wua, S. J. Xiao, *Appl. Surf. Sci.* **2010**, *256*, 4048–4051.
[58] F. Johansson, W. Hallstrom, P. Gustavsson, L. Wallman, C. Prinz, L. Montelius, M. Kanje, *J. Vac. Sci. Technol. B* **2008**, *26*, 2558–2561.
[59] L. Chen, Z. T. Chen, J. Wang, S. J. Xiao, Z. H. Lu, Z. Z. Gu, L. Kang, J. Chen, P. H. Wu, Y. C. Tangd, J. N. Liu, *Lab Chip* **2009**, *9*, 756–760.
[60] B. S. Flavel, M. J. Sweetman, C. J. Shearer, J. G. Shapter, N. H. Voelcker, *ACS Appl. Mater.Interfaces* **2011**, *3*, 2463–2471.
[61] M. J. Sweetman, C. J. Shearer, J. G. Shapter, N. H. Voelcker, *Langmuir* **2011**, *27*, 9497–9503.
[62] R. Boukherroub, D. D. M. Wayner, D. J. Lockwood, L. T. Canham, *J. Electrochem. Soc.* **2001**, *148*, H91–H97.
[63] D. J. Gao, S. J. Xiao, B. Xia, S. Wei, J. Pei, Y. Pan, X. Z. You, Z. Z. Gu, Z. Lu, *J. Phys. Chem. B* **2005**, *109*, 20620–20628.
[64] J. E. Bateman, R. D. Eagling, D. R. Worrall, B. R. Horrocks, A. Houlton, *Angew. Chem. Int. Ed.* **1998**, *37*, 2683–2685.
[65] M. Yang, R. L. M. Teeuwen, M. Giesbers, J. Baggerman, A. Arafat, F. A. de Wolf, J. C. M. van Hest, H. Zuilhof, *Langmuir* **2008**, *24*, 7931–7938.
[66] L. C. P. M. de Smet, H. Zuilhof, E. J. R. Sudholter, G. Wittstock, M. S. Duerdin, L. H. Lie, A. Houlton, B. R. Horrocks, *Electrochim. Acta* **2002**, *47*, 2653–2663.
[67] L. D. Unsworth, H. Sheardown, J. L. Brash, *Langmuir* **2008**, *24*, 1924–1929.
[68] K. A. Kilian, T. Böcking, S. Ilyas, K. Gaus, W. Jessup, M. Gal, J. J. Gooding, *Adv. Func. Mater.* **2007**, *17*, 7.
[69] A. L. Hook, H. Thissen, N. H. Voelcker, *Trends Biotechnol.* **2006**, *24*, 471–477.
[70] R. Pankov, K. M. Yamada, *J. Cell Sci.* **2002**, *115*, 3861–3863.
[71] A. Ruiz, M. Zychowicz, L. Buzanska, D. Mehn, C. A. Mills, E. Martinez, S. Coecke, J. Samitier, P. Colpo, F. Rossi, *Micro and Nanosyst.* **2009**, *1*, 50–56.
[72] A. L. Hook, H. Thissen, N. H. Voelcker, *Biomacromolecules* **2009**, *10*, 573–579.
[73] W. L. F. Armarego, D. D. Perrin, in *Purification of Laboratory Chemicals,* Butterworth-Heinemann, Oxford **1996**, pp. 529.
[74] M. Ronci, S. Sharma, T. Chataway, K. P. Burdon, S. Martin, J. E. Craig, N. H. Voelcker, *J. Proteome Res.* **2011**, *10*, 3522–3529.